


Twisted states in low-dimensional hypercubic lattices

Seungjae Lee,¹ Young Sul Cho,^{1,2,*} and Hyunsuk Hong^{1,2,†}

¹*Department of Physics, Chonbuk National University, Jeonju 54896, Korea*

²*Research Institute of Physics and Chemistry, Chonbuk National University, Jeonju 54896, Korea*

 (Received 24 February 2018; revised manuscript received 5 October 2018; published 27 December 2018)

Twisted states with nonzero winding numbers composed of sinusoidally coupled identical oscillators have been observed in a ring. The phase of each oscillator in these states constantly shifts, following its preceding neighbor in a clockwise direction, and the summation of such phase shifts around the ring over 2π characterizes the winding number of each state. In this work, we consider finite-sized d -dimensional hypercubic lattices, namely, square ($d = 2$) and cubic ($d = 3$) lattices with periodic boundary conditions. For identical oscillators, we observe new states in which the oscillators belonging to each line (plane) for $d = 2$ ($d = 3$) are phase synchronized with nonzero winding numbers along the perpendicular direction. These states can be reduced into twisted states in a ring with the same winding number if we regard each subset of phase-synchronized oscillators as one single oscillator. For nonidentical oscillators with heterogeneous natural frequencies, we observe similar patterns with slightly heterogeneous phases in each line ($d = 2$) and plane ($d = 3$). We show that these states generally appear for random configurations when the global coupling strength is larger than the critical values for the states.

DOI: [10.1103/PhysRevE.98.062221](https://doi.org/10.1103/PhysRevE.98.062221)

I. INTRODUCTION

Synchronization phenomena have been widely observed in a variety of real systems, such as flashing fireflies, cardiac pacemaker cells in the heart, firing neurons in the brain, coupled laser systems, electric power grids, hand clapping in concert halls, and Josephson junctions, among others [1–12]. The spontaneous emergence of synchronization has attracted immense interest in not only physics and biology but also many other related fields, and extensive studies have sought to understand the underlying mechanism of the phenomenon [13]. As a result, the collective properties, features, and mechanism of synchronization have been unveiled, with diverse patterns of synchronization and the origins of such patterns found [14].

One representative dynamical system is the Kuramoto model, which describes the spontaneous emergence of synchronization in a network of interacting oscillators [15]. In this system, each oscillator has a natural frequency randomly assigned from probability distribution $g(\omega)$, and the strength of coupling between each pair of connected oscillators that induces synchronization is controlled globally via control parameter K . It is known that order parameter $R > 0$ for $K > K_c [= 2/[\pi g(0)]]$ in an all-to-all coupled network structure (mean-field limit) of infinite system size [15,16]; however, $K_c \rightarrow \infty$ as system size increases to infinity in d -dimensional hypercubic lattices with Gaussian distribution $g(\omega)$ for $d \leq 4$ [17]. These results claim that low-dimensional hypercubic lattices of $d \leq 4$ can be distinct from the mean-field limit.

In ($d = 1$)-dimensional hypercubic lattices with periodic boundary conditions, regarded as ring structures, diverse multistable states have been reported [18–24]. Among these states, so-called twisted states composed of identical oscillators were found in Refs. [18,19]. In this paper, we focus on whether such twisted-state patterns can also be observed in the low-dimensional hypercubic lattices of $d = 2$ and 3, which are distinct from the mean-field limit. In addition, we explore whether similar states are possible by using Gaussian distribution $g(\omega)$ to include heterogeneity.

The rest of this paper is organized as follows. In Sec. II we introduce the general system considered in this paper. In Sec. III we review the twisted states in the ring and observe states of the same pattern in d -dimensional hypercubic lattices with periodic boundary conditions for $d = 2$ and 3. In Sec. IV we consider nonidentical oscillators with heterogeneous natural frequencies of Gaussian distribution, where we observe similar states defined by the winding number of a cycle and numerically check whether these states generally appear for random configurations. We summarize the results in Sec. V and provide details supporting our analysis in the Appendix.

II. MODEL

We study a Kuramoto system composed of N oscillators whose phases $\phi_i \in [0, 2\pi)$ ($i = 1, \dots, N$) follow the governing equation

$$\frac{d\phi_i}{dt} = \omega_i + K \sum_{j=1}^N A_{ij} \sin(\phi_j - \phi_i) \quad (1)$$

for $K > 0$, where $A_{ij} = 1$ if i and j are connected or 0 otherwise, and ω_i is the natural frequency of oscillator i .

*yscho@jbnu.ac.kr

†hhong@jbnu.ac.kr

For phase ordering, we use the order parameter given by $R = \frac{1}{N} |\sum_{j=1}^N e^{i\phi_j}|$.

In this paper, we consider d -dimensional hypercubic lattices for $d = 2$ and 3 of linear size $L = N^{1/d}$ with *periodic boundary conditions*. To specify each node in the lattices, we use a Cartesian coordinate system as follows. For a given hypercubic lattice, we choose one corner of the lattice as the origin and then define d mutually perpendicular axes, which start from the origin and increase along its d nearest neighbors. With these axes, the location of each node can be specified using d coordinates denoted by (x_1, \dots, x_d) . Here non-negative integers for x_1, \dots, x_d satisfy $0 \leq x_1, \dots, x_d \leq L - 1$.

Each node at location (x_1, \dots, x_d) is numbered by $i = \sum_{d'=1}^d x_{d'} L^{d'-1} + 1$, which makes it possible to analytically describe the states that we observe, as discussed later. We note that each positive integer i ($1 \leq i \leq N$) specifies a unique location in a given lattice. In d -dimensional hypercubic lattices with periodic boundary conditions, each node at location (x_1, \dots, x_d) is connected with $2 \times d$ nodes at locations $((x_1 \pm 1) \bmod L, \dots, x_d), \dots, (x_1, \dots, (x_d \pm 1) \bmod L)$.

III. IDENTICAL OSCILLATORS

In this section, we consider N identical oscillators with $\omega_i = \omega$ for $\forall i$. If we use a rotating reference frame $\phi_i \rightarrow \phi_i + \omega t$, Eq. (1) takes the form

$$\frac{d\phi_i}{dt} = K \sum_{j=1}^N A_{ij} \sin(\phi_j - \phi_i). \quad (2)$$

A. Twisted state on a ring

The twisted state on a ring structure composed of identical oscillators was originally reported in Ref. [18]. For the ring structure, Eq. (2) has the form

$$\frac{d\phi_i}{dt} = K [\sin(\phi_{i-1} - \phi_i) + \sin(\phi_{i+1} - \phi_i)] \quad (3)$$

with $\phi_{N+1} \equiv \phi_1$ and $\phi_0 \equiv \phi_N$. In a twisted state of integer winding number q (q -twisted state), the phases of the oscillators are $\phi_i = (2\pi qi/N + C) \bmod 2\pi$ for any constant C .

It can be shown that this state is a *fully phase-locked* state ($\dot{\phi}_i = 0$ for $\forall i$) by substituting this form into the right-hand side of Eq. (3). Moreover, it has been proven that this state is linearly stable for $N > 4|q|$ [18,19]. Here q is called the winding number because this value refers to the number of full twists of the phase around the ring. We discuss the definition of winding number for an arbitrary cycle within the given network structure in Sec. IV A [20–24].

B. Twisted states in d -dimensional hypercubic lattices for $d = 2$ and 3

We observe similar states in d -dimensional hypercubic lattices for $d = 2$ and 3 . In these states, the oscillators in each line (plane) for $d = 2$ ($d = 3$) are phase synchronized, while the phase of each line (plane) is constantly shifted by $2\pi q/L$ from that of the preceding line (plane) along the perpendicular axis.

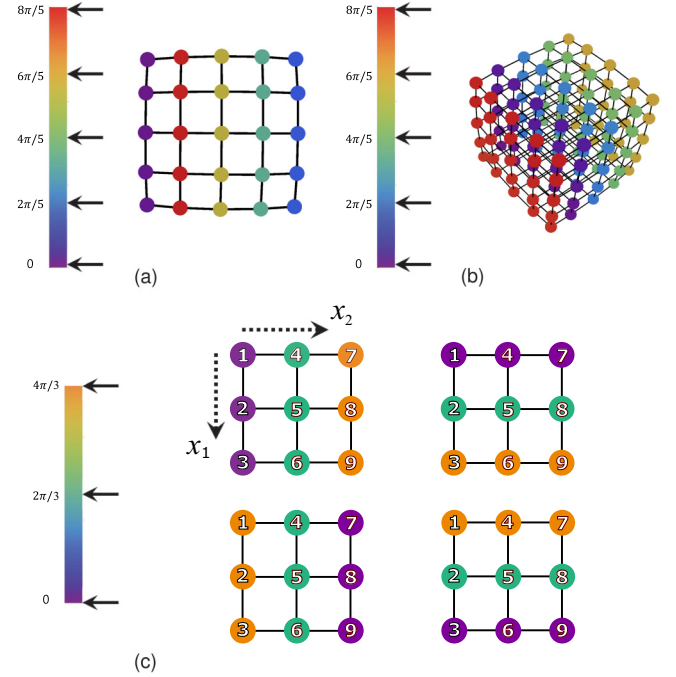


FIG. 1. (a, b) Schematic diagram for the ($q = 1$)-twisted states in (a) two- and (b) three-dimensional hypercubic lattices for $L = 3$. The phase of each oscillator is denoted by the corresponding color of the palette on the left. The oscillators belonging to each column have the same phases in (a), and the oscillators belonging to each plane have the same phases in (b). Arrows are continually shifted upward by $2\pi/L$ starting from the bottom value 0. (c) Schematic diagram of $2 \times d = 4$ numbers of different patterns of ($q = 1$)-twisted states for a fixed coordinate system (dotted arrows) in a two-dimensional hypercubic lattice with $L = 3$. The phase of each oscillator is denoted by the corresponding color of the palette on the left. Solid arrows are continually shifted upward by $2\pi/L$ starting from the bottom value 0. (a–c) We note that links between pairs of nodes on opposite sides are omitted.

By translating and rotating the coordinate axes (renumbering the nodes following the rule in the last paragraph of Sec. II), we can formulate these states as

$$\phi_i^* = \left(\frac{2\pi q}{L} \left\lfloor \frac{i-1}{L^{d-1}} \right\rfloor + C \right) \bmod 2\pi \quad (4)$$

for any constant C with non-negative integer $q \geq 0$, where $\lfloor x \rfloor$ denotes the integer part of a given number x . We note that the x_d axis is used for the direction of non-negative winding number q . We consider $0 \leq q \leq \lfloor L/2 \rfloor$ by using the restriction of the phase difference $(2\pi q/L) \in [0, \pi]$. We call these states *q-twisted states* (in d -dimensional hypercubic lattices) because these states can be reduced to q -twisted states on a ring of size L if we regard each subset of phase-synchronized oscillators as one single oscillator with the same phase. A schematic diagram for these states with $q = 1$ is shown in Figs. 1(a) and 1(b). We remark that all $2 \times d$ numbers of different patterns with the same $q > 0$ value for a fixed coordinate system driven by rotational and reflectional symmetry are regarded as q -twisted states [Fig. 1(c)].

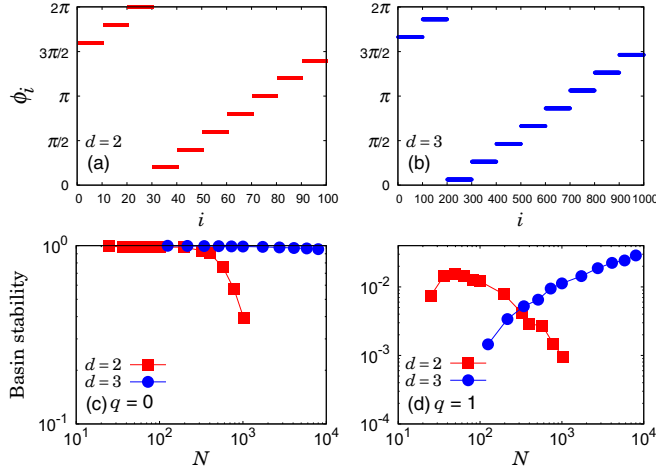


FIG. 2. Two configurations of numerically obtained ($q = 1$)-twisted states for (a) $d = 2$ and (b) $d = 3$ of $L = 10$. Numerically measured basin stability of the twisted states of (c) $q = 0$ and (d) $q = 1$ for both $d = 2$ and $d = 3$ for various N . We use 10^5 random initial conditions with $K = 5.0$ for each N . We note that the result for a single K value is sufficient because K changes the timescale only in Eq. (2).

We show that the q -twisted state of the form Eq. (4) is a fully phase-locked state of Eq. (2) in general d -dimensional hypercubic lattices. This can be proved by inserting this form directly into the right-hand side of Eq. (2), which gives $K \sin(\phi_{i+L^{d-1}}^* - \phi_i^*) + K \sin(\phi_{i-L^{d-1}}^* - \phi_i^*) = K \sin(2\pi q/L) - K \sin(2\pi q/L) = 0$.

Then we show that this state is linearly stable for $L > 4q$. For small deviations from the twisted state, $\phi_i = \phi_i^* + \delta\phi_i$, the rate equation for $\delta\phi_i$ up to linear order is derived as

$$\delta\dot{\phi}_i = \sum_j J_{ij} \delta\phi_j, \quad (5)$$

where Jacobian matrix $J_{ij} \equiv \left. \frac{\partial \dot{\phi}_i}{\partial \phi_j} \right|_{\phi=\phi^*}$ is given as

$$J_{ij} = \begin{cases} -K \sum_{k=1}^N A_{ik} \cos(\phi_k^* - \phi_i^*) & \text{if } j = i, \\ K A_{ij} \cos(\phi_j^* - \phi_i^*) & \text{if } j \neq i. \end{cases} \quad (6)$$

To investigate the linear stability of the twisted state, we obtain the eigenvalues of the Jacobian matrix. For $L > 4q$, we find that all eigenvalues are negative except for one zero, which is related to perturbation within the manifold. Therefore, the twisted state is linearly stable for $L > 4q$. For $L = 4q$, multiplicity of the zero eigenvalue is larger than one, and the other eigenvalues are negative, which means that the twisted state is neutrally stable. For $L < 4q$, we find that some eigenvalues are positive, and thus the twisted state is unstable [25,26] (see Sec. 1 in the Appendix).

We observe twisted states of $q = 1$ for $d = 2$ and 3 by numerical simulations for randomly given initial phases $\phi_i(0) \in [0, 2\pi)$ for $\forall i$, as shown in Figs. 2(a) and 2(b). To confirm that the emergence of these twisted states is not the result of particular choices of initial phases, we measure the fraction of random initial conditions that induces the twisted states (referred to as the *basin stability* of the twisted states [27]); specifically, we begin with a set of random initial

phases $\phi_i(0) \in [0, 2\pi)$ for $\forall i$ for each configuration. We test a large number of configurations by changing the initial phases for different configurations, and then obtain the fraction of configurations that arrives at the q -twisted states (basin stability of the q -twisted states) for each q value separately. The results for $q = 0$ and $q = 1$ are shown in Figs. 2(c) and 2(d), respectively. We could not observe the twisted states for $1 < q < L/4$ numerically, even though the states are linearly stable. This might be because the basin stability of the q -twisted states for $1 < q < L/4$ are so small.

It should be noted that, for the emergence of twisted states, each pair of oscillators on opposite sides should be synchronized, and therefore the periodic boundary conditions here are important because they allow for direct coupling between the oscillators in each pair.

Now, we are curious about the spontaneous synchronization of the oscillators in each line ($d = 2$) or in each plane ($d = 3$), which seems unnatural considering the rotational symmetry of the hypercubic lattice. We find that, in fact, such patterns originate from the translational symmetry of the hypercubic lattice [28]. More precisely, we use automorphism, which is a permutation of the nodes preserving the adjacency matrix. In Refs. [29–32] it was reported that each set of nodes that permute to each other by an automorphism (mathematical) group can be synchronized. Based on such results, we show that synchronization of each line (plane) requires the synchronizations of all the others, such that every line (plane) is synchronized at the same time (see Sec. 2 in the Appendix). Therefore, we expect that twisted states would be observed in other lattices that include translational symmetry, for example, hypercubic lattices for $d > 3$.

IV. NONIDENTICAL OSCILLATORS

In this section, we consider the Gaussian distribution function $g(\omega)$ with zero mean and arbitrary variances. We choose ω_i randomly from a certain $g(\omega)$. To be specific, we choose a set $\{\omega_i\}_{1 \leq i \leq N}$ for the given $g(\omega)$ and N by using the relation

$$\tilde{\sigma}(i) = \frac{1}{2} + N \int_{-\infty}^{\omega_i} g(\omega) d\omega, \quad (7)$$

where $\tilde{\sigma}$ is a random permutation of the set $\{1, 2, \dots, N\}$. This method gives $\sum_{i=1}^N \omega_i = 0$ exactly [33].

A. Winding number of a cycle

To find the winding number of a cycle, we consider an arbitrary cycle denoted by c of length n in the given network structure. The sequence of nodes of cycle c is given by (c_0, \dots, c_{n-1}) . Then the winding number of c is given by $q(c) = (2\pi)^{-1} \sum_{i=0}^{n-1} \Delta_{i+1,i}$, where $\Delta_{i+1,i} = (\phi_{c_{i+1}} - \phi_{c_i}) \bmod 2\pi \in (-\pi, \pi]$ with $c_n \equiv c_0$. For dynamical systems with Eq. (1), $q(c)$ must be an integer [23].

B. States with nonzero winding numbers along only one axis for $d = 2$ and 3

For a d -dimensional hypercubic lattice with periodic boundary conditions composed of nonidentical oscillators, we again consider the coordinate system introduced in Sec. II.

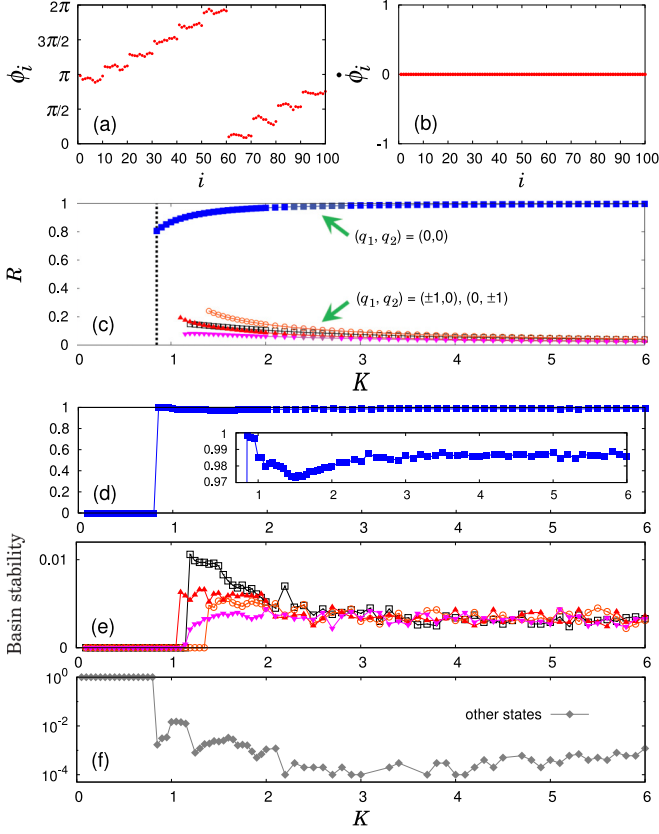


FIG. 3. Data for a two-dimensional hypercubic lattice of $L = 10$ for a randomly given set $\{\omega_i\}_{1 \leq i \leq N}$ with unit variance, obtained by numerically integrating Eq. (1) up to $t = 10^3$. (a) ϕ_i vs i for a numerically obtained state with $(q_1, q_2) = (1, 0)$. (b) Confirmation that the state in panel (a) is a fully phase-locked state. (c) Average value of R over the numerically obtained states for pairs $(q_1, q_2) = (0, 0)$ (■), $(1, 0)$ (□), $(-1, 0)$ (○), $(0, 1)$ (▲), and $(0, -1)$ (▼) for each value of K . In the range of K to the left of the vertical dotted line, we cannot obtain any fully phase-locked states. (d–f) Numerically measured basin stabilities of states for pairs (d) $(q_1, q_2) = (0, 0)$, (e) $(\pm 1, 0)$ and $(0, \pm 1)$, and (f) other states using 10^4 random initial conditions for each value of K . The inset in panel (d) is an enlarged plot of R vs K in the main panel. The symbols in panels (d) and (e) are the same as in panel (c) to denote (q_1, q_2) .

For $d = 2$ and 3 , we observe fully phased-locked states that show the same behavior as the $(q = 1)$ -twisted states from the perspective of winding numbers. However, each ϕ_i in these states is slightly perturbed from Eq. (4) in general by the heterogeneous natural frequencies. We demonstrate these states in $d = 2$ and $d = 3$ lattices separately.

For $d = 2$, we fix a two-dimensional coordinate system and then use notations $c^{(x_1, 0)}$ and $c^{(0, x_2)}$ for the cycles with sequences of nodes $(c_{x_2}^{(x_1, 0)})_{x_2=0}^{L-1}$ and $(c_{x_1}^{(0, x_2)})_{x_1=0}^{L-1}$. Here both $c_{x_2}^{(x_1, 0)}$ and $c_{x_1}^{(0, x_2)}$ denote the node at location (x_1, x_2) . Therefore, each cycle $c^{(x_1, 0)}$ can be regarded as a sequence of nodes reachable from $(x_1, 0)$ using links along the x_2 axis. Similarly, each cycle $c^{(0, x_2)}$ can be regarded as a sequence of nodes reachable from $(0, x_2)$ by paths along the x_1 axis. We note that each sequence in $c^{(x_1, 0)}$ and $c^{(0, x_2)}$ forms a cycle by a link connecting the two ends from the periodic boundary conditions.

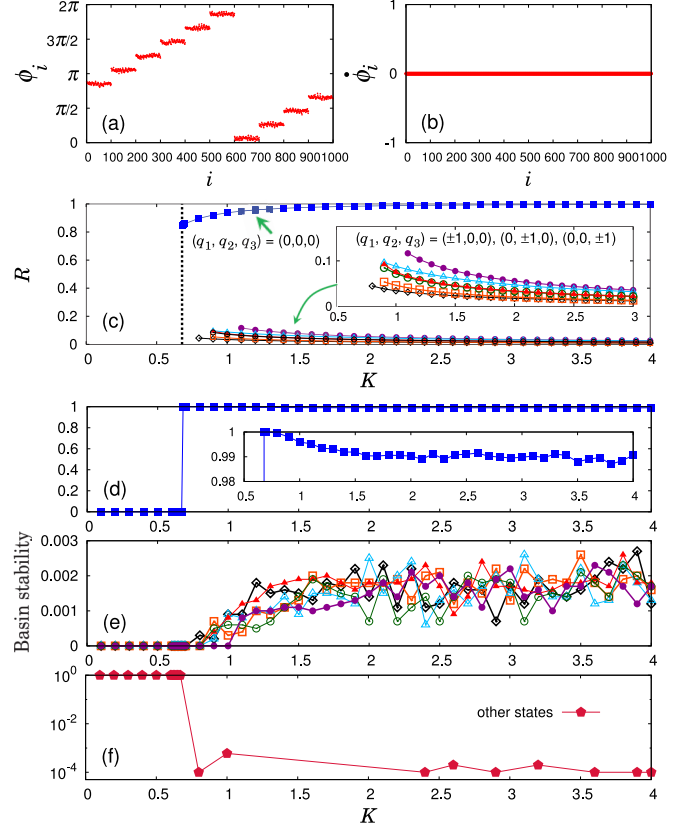


FIG. 4. Data for a three-dimensional hypercubic lattice of $L = 10$ for a randomly given set $\{\omega_i\}_{1 \leq i \leq N}$ with unit variance, obtained by numerically integrating Eq. (1) up to $t = 5 \times 10^2$. (a) ϕ_i vs i for a numerically obtained state with $(q_1, q_2, q_3) = (1, 0, 0)$. (b) Confirmation that the state in (a) is a fully phase-locked state. (c) Average value of R over the numerically obtained states for $(q_1, q_2, q_3) = (0, 0, 0)$ (■), $(1, 0, 0)$ (◊), $(-1, 0, 0)$ (□), $(0, 1, 0)$ (●), $(0, -1, 0)$ (△), $(0, 0, 1)$ (▲), and $(0, 0, -1)$ (○) for each value of K . In the range of K to the left of the vertical dotted line, we cannot obtain any fully phase-locked states. Inset: Enlarged plot of R vs K in the main panel. (d–f) Numerically measured basin stabilities of states for (d) $(q_1, q_2, q_3) = (0, 0, 0)$, (e) $(\pm 1, 0, 0)$, $(0, \pm 1, 0)$, and $(0, 0, \pm 1)$, and (f) other states using 10^4 random initial conditions for each value of K . The inset in panel (d) is an enlarged plot of R vs K in the main panel. The symbols in panels (d) and (e) are the same as in panel (c) to denote (q_1, q_2, q_3) .

We observe fully phase-locked states where $q(c^{(x_1, 0)}) = q_1$ for $\forall x_1$ and $q(c^{(0, x_2)}) = q_2$ for $\forall x_2$ for five different pairs: $(q_1, q_2) = (0, 0)$, $(\pm 1, 0)$, and $(0, \pm 1)$. Interestingly, for $d = 2$, $(q_1, q_2) = (0, 0)$ is a characteristic of the $(q = 0)$ -twisted states, while the other four pairs are characteristics of the $(q = 1)$ -twisted states. We measure the basin stability of the states in each (q_1, q_2) pair separately for a randomly given set, $\{\omega_i\}_{1 \leq i \leq N}$, as shown in Fig. 3. The numerical results support that each pair can be observed when K is larger than each critical value of K . We obtained similar results for 10 different randomly given sets $\{\omega_i\}_{1 \leq i \leq N}$.

For $d = 3$, we fix a three-dimensional coordinate system and then use notations $c^{(x_1, x_2, 0)}$, $c^{(x_1, 0, x_3)}$, and $c^{(0, x_2, x_3)}$ for the cycles with sequences of nodes $(c_{x_3}^{(x_1, x_2, 0)})_{x_3=0}^{L-1}$, $(c_{x_2}^{(x_1, 0, x_3)})_{x_2=0}^{L-1}$, and $(c_{x_1}^{(0, x_2, x_3)})_{x_1=0}^{L-1}$, respectively. Here $c_{x_3}^{(x_1, x_2, 0)}$, $c_{x_2}^{(x_1, 0, x_3)}$, and

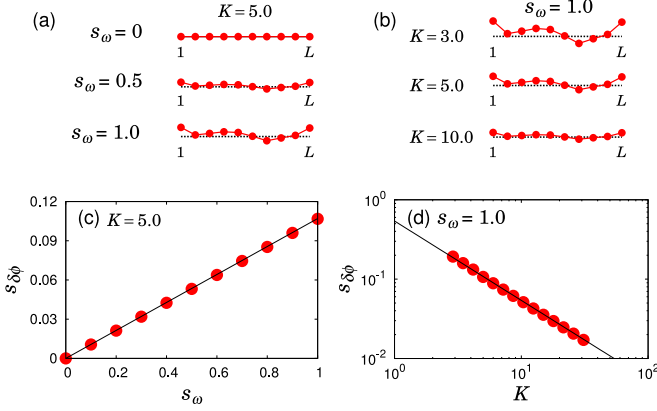


FIG. 5. ϕ_i (\bullet) near ϕ_i^* (dotted line) of states with $(q_1, q_2) = (1, 0)$ in a line in a two-dimensional lattice of $L = 10$ for (a) changing s_ω with fixed $K = 5.0$ and (b) changing K with fixed $s_\omega = 1.0$. The height of each circle denotes ϕ_i of corresponding i , with the same scale for the difference of ϕ to the corresponding difference of height used for all pairs of (s_ω, K) in panels (a) and (b). We find that deviation from the straight form increases as s_ω increases for fixed K in (a), while it decreases as K increases for fixed s_ω in panel (b). Note that the dotted line for $s_\omega = 0$ in panel (a) is hidden because $\phi_i = \phi_i^*$ exactly. (c, d) Numerically obtained (c) $s_{\delta\phi}$ vs s_ω for fixed $K = 5.0$, and (d) $s_{\delta\phi}$ vs K for fixed $s_\omega = 1.0$. In both panels (c) and (d), a two-dimensional lattice of $L = 10$ is used. Solid lines are eye guides to show the relation $s_{\delta\phi} \propto s_\omega/K$.

$c_{x_1}^{(0, x_2, x_3)}$ denote the node at location (x_1, x_2, x_3) . We observe fully phase-locked states where $q(c^{(x_1, x_2, 0)}) = q_1$ for $\forall x_1, x_2$, $q(c^{(x_1, 0, x_3)}) = q_2$ for $\forall x_1, x_3$, and $q(c^{(0, x_2, x_3)}) = q_3$ for $\forall x_2, x_3$ for seven different sets: $(q_1, q_2, q_3) = (0, 0, 0)$, $(\pm 1, 0, 0)$, $(0, \pm 1, 0)$, and $(0, 0, \pm 1)$. Similar to the previous case, $(q_1, q_2, q_3) = (0, 0, 0)$ is a characteristic of the $(q = 0)$ -twisted states for $d = 3$, while the other six sets are characteristics of the $(q = 1)$ -twisted states. We measure the basin stability of the states in each (q_1, q_2, q_3) set separately for a randomly given set $\{\omega_i\}_{1 \leq i \leq N}$, with results shown in Fig. 4. The numerical results again support that each set can be observed when K is larger than each critical value of K . We obtained similar results for 10 different randomly given sets $\{\omega_i\}_{1 \leq i \leq N}$.

In contrast to Figs. 2(a) and 2(b), where ϕ_i vs i of each $(q = 1)$ -twisted state shows a clear shape, which looks like evenly spaced stairs, ϕ_i vs i of the states composed of nonidentical oscillators with $(q_1, q_2) = (1, 0)$ in Fig. 3(a) and $(q_1, q_2, q_3) = (1, 0, 0)$ in Fig. 4(a) have roughness. We ascertain that the slightly heterogeneous phases in each line [Fig. 3(a)] and plane [Fig. 4(a)] of the two states originate from the heterogeneity of the natural frequencies.

We now consider small deviations from the q -twisted state given by $\delta\phi_i = \phi_i - \phi_i^*$ with $|\delta\phi_i| \ll 1$ for $\forall i$. Then $\delta\phi_i$ in a fully phase-locked state (i.e., $\phi_i = \delta\phi_i = 0$ for $\forall i$) follows

$$\omega_i = - \sum_{j=1}^N J_{ij} \delta\phi_j. \quad (8)$$

This allows us to show that $s_{\delta\phi} \propto s_\omega/K$ analytically, where s_x is the standard deviation of the set $\{x_i\}_{1 \leq i \leq N}$. Here

$s_{\delta\phi} = \sqrt{\sum_{i=1}^N \delta\phi_i^2 / N}$ by using the constraint $\sum_{i=1}^N \delta\phi_i = 0$, because $\sum_{i=1}^N \delta\phi_i$ can have any value by the singularity of the Jacobian matrix (see Sec. 3 in the Appendix). We note that $s_\omega = \sqrt{\sum_{i=1}^N \omega_i^2 / N}$ by $\sum_{i=1}^N \omega_i = 0$, which is the result of Eq. (7). This result supports that roughness arises due to the heterogeneity of the natural frequencies. We check $s_{\delta\phi} \propto s_\omega/K$ via numerical simulation as shown in Fig. 5.

The result of the preceding paragraph claims that states with $(q_1, q_2) = (\pm 1, 0)$, $(0, \pm 1)$ for $d = 2$ and $(q_1, q_2, q_3) = (\pm 1, 0, 0)$, $(0, \pm 1, 0)$, $(0, 0, \pm 1)$ for $d = 3$ would become $(q = 1)$ -twisted states as $K \rightarrow \infty$ for a fixed s_ω . Twisted states of $q > 0$ have $R = 0$ exactly; consequently, R of the states with these pairs of (q_1, q_2) and sets of (q_1, q_2, q_3) decrease to zero, as seen in Fig. 3(c) and Fig. 4(c).

V. SUMMARY

In summary, we studied a Kuramoto model [Eq. (1)] in two- and three-dimensional hypercubic lattices with periodic boundary conditions. For identical oscillators in two (three) dimensions, we observed fully phase-locked states where oscillators in each line (plane) are phase synchronized, and the phase of each line (plane) is constantly shifted by $2\pi/L$ from that of its preceding line (plane) along the perpendicular axis. For heterogeneous, natural frequencies given by a Gaussian distribution function, similar patterns with slightly heterogeneous phases in each line (plane) were observed in two (three) dimensions. We measured the basin stability of these states and conclude that such states generally appear when K is larger than their critical values of K .

In a previous study [17], the same system was studied using the ‘‘annealed or adiabatic’’ initial condition. Initial phases in such a condition for each K are not given randomly, but rather the phases of the steady state of the preceding K value are used successively. Therefore, the states found in this current work may not have been observed.

ACKNOWLEDGMENT

This work was supported by NRF Grants No. 2017R1C1B1004292 (Y.S.C.) and No. 2018R1A2B6001790 (H.H.).

APPENDIX

1. Spectral properties of the Jacobian matrix to explain that the q -twisted state is stable only when $L > 4q$

In this section we derive some spectral properties of the Jacobian matrix to determine whether the q -twisted state is linearly stable or not depending on L . We can obtain the Jacobian matrix for the twisted states by applying the definition $J_{ij} \equiv \left. \frac{\partial \phi_i}{\partial \phi_j} \right|_{\phi=\phi^*}$ to Eq. (2), as

$$\begin{aligned} J_{ij} &\equiv \left. \frac{\partial \phi_i}{\partial \phi_j} \right|_{\phi=\phi^*} = \frac{\partial}{\partial \phi_j} \left[K \sum_{k=1}^N A_{ik} \sin(\phi_k - \phi_i) \right] \Big|_{\phi=\phi^*} \\ &= K \sum_{k=1}^N A_{ik} \cos(\phi_k - \phi_i) (\delta_{kj} - \delta_{ij}) \Big|_{\phi=\phi^*} \end{aligned}$$

$$\begin{aligned}
&= K A_{ij} \cos(\phi_j^* - \phi_i^*) - \delta_{ij} K \sum_{k=1}^N A_{ik} \cos(\phi_k^* - \phi_i^*) \\
&= \begin{cases} -K \sum_{k=1}^N A_{ik} \cos(\phi_k^* - \phi_i^*) & \text{if } j = i, \\ K A_{ij} \cos(\phi_j^* - \phi_i^*) & \text{if } j \neq i. \end{cases} \quad (\text{A1})
\end{aligned}$$

From Eq. (A1), we can confirm that $J_{ij} = J_{ji}$, or in other words, \mathbf{J} is a real symmetric matrix. Therefore, \mathbf{J} is orthogonally diagonalizable. In order to investigate the linear stability of the q -twisted state, we need to obtain some information on the eigenvalues of the Jacobian matrix.

a. Nonpositive eigenvalues in the Jacobian matrix for $L \geq 4q$

We show that the Jacobian matrix for $L \geq 4q$ is a negative semidefinite matrix whose eigenvalues are non-positive. The incidence matrix \mathbf{M} is a $Nd \times N$ matrix whose elements are $M_{ei} = \sqrt{K A_{ij} \cos(\phi_j^* - \phi_i^*)}$ and $M_{ej} = -\sqrt{K A_{ij} \cos(\phi_j^* - \phi_i^*)}$ if e connects two nodes i and j but 0 otherwise. From the definition of the incidence matrix, we can derive

$$\begin{aligned}
[\mathbf{M}^T \mathbf{M}]_{ii} &= \sum_{e=1}^{Nd} (M_{ei})^2 = \sum_{j=1}^N K A_{ij} \cos(\phi_j^* - \phi_i^*) = -J_{ii}, \\
[\mathbf{M}^T \mathbf{M}]_{ij} &= \sum_{e=1}^{Nd} M_{ei} M_{ej} = -K A_{ij} \cos(\phi_j^* - \phi_i^*) = -J_{ij}.
\end{aligned} \quad (\text{A2})$$

From Eq. (A2), $\mathbf{J} = -\mathbf{M}^T \mathbf{M}$. If we use \mathbf{v}_i and λ_i for the i th eigenvector and eigenvalue of \mathbf{J} , $\mathbf{J} \mathbf{v}_i = \lambda_i \mathbf{v}_i$ for $i = 1, \dots, N$. Here \mathbf{v}_i are real vectors and λ_i are real values because \mathbf{J} is orthogonally diagonalizable. Then $\lambda_i = \mathbf{v}_i^T \mathbf{J} \mathbf{v}_i = -\mathbf{v}_i^T \mathbf{M}^T \mathbf{M} \mathbf{v}_i = -|\mathbf{M} \mathbf{v}_i|^2 \leq 0$ for \forall_i when $L \geq 4q$. We remark that this is not applicable for $L < 4q$ (i.e., $L/4 < q \leq \lfloor L/2 \rfloor$) because some elements of \mathbf{M} , $\sqrt{K \cos(2\pi q/L)}$ are imaginary numbers. Therefore, \mathbf{J} for $L \geq 4q$ is a negative semidefinite matrix and its eigenvalues are nonpositive.

b. Zero eigenvalue of multiplicity one for $L > 4q$ and multiplicity L for $L = 4q$ in the Jacobian matrix

In this subsection, we consider negative semidefinite matrix \mathbf{J} for $L \geq 4q$. \mathbf{J} has at least one eigenvalue of 0 related to stability for the perturbation of constant phase shifts for all oscillators. Therefore, the twisted state is stable if the multiplicity of eigenvalue 0 is one, but the twisted state is neutrally stable if the multiplicity of eigenvalue 0 is larger than one. We show that the twisted state is stable for $L > 4q$ and neutrally stable for $L = 4q$ by investigating the multiplicity in each case.

For the analysis, we decompose the hypercubic lattice into two subnetworks whose adjacency matrices are denoted by $\mathbf{A}^{(1)}$ and $\mathbf{A}^{(2)}$. The first subnetwork consists of $2(d-1)N$ number of links parallel to the $x_{d'}$ axis for $1 \leq d' \leq d-1$, and the second subnetwork consists of the other $2N$ number of links parallel to the x_d axis. Then \mathbf{J} is decomposed into two terms as

$$\mathbf{J} = -K \mathbf{L}^{(1)} - K \cos\left(\frac{2\pi q}{L}\right) \mathbf{L}^{(2)}, \quad (\text{A3})$$

where $\mathbf{L}^{(1)}$ and $\mathbf{L}^{(2)}$ are the Laplacian matrices of $\mathbf{A}^{(1)}$ and $\mathbf{A}^{(2)}$, respectively.

When $L = 4q$, the Jacobian matrix is reduced to $\mathbf{J} = -K \mathbf{L}^{(1)}$. It is known that the multiplicity of the eigenvalue 0 in a Laplacian matrix is equal to the number of connected components in the given network. The number of connected components in $\mathbf{A}^{(1)}$ is L , which clarifies that the multiplicity of eigenvalue 0 is $L = 4q$. Therefore, the twisted state for $L = 4q$ is neutrally stable.

On the other hand, when $L > 4q$ we show that the multiplicity of eigenvalue 0 is one by way of contradiction. We assume that eigenvalue 0 has two linearly independent eigenvectors \mathbf{v}_1 and \mathbf{v}_2 . Then

$$\begin{aligned}
0 &= \mathbf{v}_1^T \mathbf{J} \mathbf{v}_1 = -\mathbf{v}_1^T \left[K \mathbf{L}^{(1)} + K \cos\left(\frac{2\pi q}{L}\right) \mathbf{L}^{(2)} \right] \mathbf{v}_1 \\
&= -K \mathbf{v}_1^T \mathbf{L}^{(1)} \mathbf{v}_1 - K \cos\left(\frac{2\pi q}{L}\right) \mathbf{v}_1^T \mathbf{L}^{(2)} \mathbf{v}_1 \\
&= -\frac{K}{2} \sum_{i,j=1}^N A_{ij}^{(1)} (v_{1i} - v_{1j})^2 \\
&\quad - \frac{K}{2} \cos\left(\frac{2\pi q}{L}\right) \sum_{i,j=1}^N A_{ij}^{(2)} (v_{1i} - v_{1j})^2 = 0. \quad (\text{A4})
\end{aligned}$$

Since each term in the summations is positive, i.e., \mathbf{v}_1 is a real vector because \mathbf{J} is orthogonally diagonalizable, each term should be zero. Thus, $v_{1i} = v_{1j}$ for $\forall_{i,j}$ because all the oscillators belong to one connected component for $\mathbf{A} = \mathbf{A}^{(1)} + \mathbf{A}^{(2)}$. In the same way, we can obtain $v_{2i} = v_{2j}$ for $\forall_{i,j}$, which tells us that \mathbf{v}_2 is a scalar multiplication of \mathbf{v}_1 . This violates the assumption that \mathbf{v}_1 and \mathbf{v}_2 are linearly independent, thereby proving that multiplicity of eigenvalue 0 is one for $L > 4q$. Therefore, the twisted state for $L > 4q$ is stable.

c. Positive eigenvalues in the Jacobian matrix for $L < 4q$

In this subsection, we show that at least $(L-1)$ eigenvalues of \mathbf{J} for $L < 4q$ are positive. We consider $N \times 1$ column vectors $\mathbf{v}^{(\ell)}$ ($\ell = 0, \dots, L-1$) where $v_i^{(\ell)} = 1/\sqrt{L^{d-1}}$ if $\lfloor (i-1)/L^{d-1} \rfloor = \ell$ and 0 otherwise. $\mathbf{v}^{(\ell)}$ is parallel to the direction of the constant phase shifts of the nodes in the ℓ th synchronized subset. Then $\mathbf{J} \mathbf{v}^{(\ell)} = -K \cos(2\pi q/L) \mathbf{L}^{(2)} \mathbf{v}^{(\ell)} = K \cos(2\pi q/L) (\mathbf{v}^{(\ell+1)} - 2\mathbf{v}^{(\ell)} + \mathbf{v}^{(\ell-1)})$ with $\mathbf{v}^{(L)} \equiv \mathbf{v}^{(0)}$ and $\mathbf{v}^{(-1)} \equiv \mathbf{v}^{(L-1)}$.

An $L \times L$ matrix $\tilde{\mathbf{J}}^{(2)}$ given by

$$\tilde{\mathbf{J}}_{mn}^{(2)} = \begin{cases} -2K \cos\left(\frac{2\pi q}{L}\right) & \text{if } n = m, \\ K \cos\left(\frac{2\pi q}{L}\right) & \text{if } n = 1 + (m \pm 1) \bmod L \\ 0 & \text{otherwise} \end{cases} \quad (\text{A5})$$

is orthogonally diagonalizable for an orthogonal matrix \mathbf{U} , such as $\mathbf{U}^T \tilde{\mathbf{J}}^{(2)} \mathbf{U} = \Lambda$ where $\Lambda_{mn} = \lambda_n \delta_{mn}$. Without a loss of generality, we set the first eigenvalue to $\lambda_1 = 0$ by fixing the first column of \mathbf{U} as $U_{m1} = \frac{1}{\sqrt{L}}$. Here $\tilde{\mathbf{J}}^{(2)} = -K \cos(2\pi q/L) \tilde{\mathbf{L}}^{(2)}$ for the Laplacian matrix of a ring of length L denoted by $\tilde{\mathbf{L}}^{(2)}$. By the property of the Laplacian matrix, $\tilde{\mathbf{L}}^{(2)}$ has one zero eigenvalue, and all the other eigenvalues are positive. Therefore, $\lambda_n > 0$

($1 < n \leq L$) for $L < 4q$. Finally, $\mathbf{J}(\sum_{m=1}^L U_{mn} \mathbf{v}^{(m-1)}) = \lambda_n(\sum_{m=1}^L U_{mn} \mathbf{v}^{(m-1)})$, which means that $\sum_{m=1}^L U_{mn} \mathbf{v}^{(m-1)}$ is an eigenvector of \mathbf{J} with the eigenvalue λ_n . Therefore, at least $(L-1)$ positive eigenvalues (i.e., λ_n for $1 < n \leq L$) of \mathbf{J} exist.

2. Symmetry-inducing synchronization of subsets in the twisted states

In this section, we analyze the relation between the automorphism and synchronization of the subset of oscillators in the twisted states for both two and three dimensions in more detail.

For $d = 2$, we consider a permutation of nodes σ given by

$$\sigma(i) = \begin{cases} i - L + 1 & \text{if } i \bmod L = 0, \\ i + 1 & \text{otherwise.} \end{cases} \quad (\text{A6})$$

Under this permutation, the adjacency matrix is preserved (i.e., $A_{ij} = A_{\sigma(i)\sigma(j)}$), which means that σ is an automorphism for $d = 2$. Then we can construct the group $G = \langle \sigma \rangle$ generated by σ . The orbit of i operated by G , denoted by $\varphi(G, i)$, is defined as $\varphi(G, i) = \{\tilde{\sigma}(i) | \tilde{\sigma} \in G\}$. By the property of the group, it is guaranteed that $\varphi(G, i) = \varphi(G, j)$ for all $j \in \varphi(G, i)$. Here $\varphi(G, i)$ is the subset of oscillators belonging to the same line with i , and all oscillators in the lattice are partitioned into a unique set of orbits $\{\varphi(G, 1), \varphi(G, L+1), \dots, \varphi(G, L(L-1)+1)\} = \{\varphi_1, \dots, \varphi_\ell, \dots, \varphi_L\}$ by G . Here reduced notation φ_ℓ denotes the subset of oscillators in the ℓ th orbit, which is the same as the subset of oscillators in the ℓ th line.

For $d = 3$, we consider two automorphisms σ_1 and σ_2 given by

$$\sigma_1(i) = \begin{cases} i - L + 1 & \text{if } i \bmod L = 0, \\ i + 1 & \text{otherwise} \end{cases}$$

and

$$\sigma_2(i) = \begin{cases} i - (L-1)L & \text{if } \{1 + (i - i \bmod L)/L\} \bmod L = 0, \\ i + L & \text{otherwise.} \end{cases}$$

For the group $G = \langle \sigma_1, \sigma_2 \rangle$ generated by σ_1 and σ_2 , all oscillators in the lattice are partitioned into a unique set of orbits $\{\varphi(G, 1), \varphi(G, L^2+1), \dots, \varphi(G, L^2(L-1)+1)\} = \{\varphi_1, \dots, \varphi_\ell, \dots, \varphi_L\}$ by G , where φ_ℓ is the same as the subset of the oscillators in the ℓ -th plane. In both dimensional cases, we consider general states where $\phi_i = s_\ell$ for $\forall i \in \varphi_\ell$ ($\ell = 1, \dots, L$). Then an arbitrary $i \in \varphi_\ell$ follows the equation

$$\dot{s}_\ell = K \sin(s_{\ell+1} - s_\ell) + K \sin(s_{\ell-1} - s_\ell). \quad (\text{A7})$$

This means that each subset of oscillators can be synchronized when all the other subsets are synchronized. In this way, symmetry can explain the simultaneous synchronizations of all subsets.

3. Derivation of $s_{\delta\phi} \propto s_\omega/K$

In this section, we derive $s_{\delta\phi} \propto s_\omega/K$ starting from $\boldsymbol{\omega} = -\mathbf{J}\delta\boldsymbol{\phi}$ [Eq. (8)], where Eq. (8) is represented by using the vectors $\boldsymbol{\omega} = (\omega_1, \dots, \omega_N)^\top$ and $\delta\boldsymbol{\phi} = (\delta\phi_1, \dots, \delta\phi_N)^\top$. We

consider \mathbf{J} for $L > 4q$. \mathbf{J} is orthogonally diagonalizable for an orthogonal matrix \mathbf{U} , such as $\mathbf{U}^\top \mathbf{J} \mathbf{U} = \boldsymbol{\Lambda}$, where $\Lambda_{ij} = \lambda_i \delta_{ij}$ and λ_i is the i th eigenvalue of \mathbf{J} . We showed that only one zero eigenvalue exists for \mathbf{J} with $L > 4q$ in Sec. 1b of the Appendix. Without a loss of generality, we set the first eigenvalue to $\lambda_1 = 0$ and $\lambda_i \neq 0$ for $i > 1$. Under these conditions, the first column of \mathbf{U} is fixed as $U_{i1} = \frac{1}{\sqrt{N}}$.

From $\boldsymbol{\omega} = -\mathbf{J}\delta\boldsymbol{\phi}$, we can derive $\mathbf{U}^\top \boldsymbol{\omega} = -\boldsymbol{\Lambda} \mathbf{U}^\top \delta\boldsymbol{\phi}$ by $\mathbf{U}^\top = \mathbf{U}^{-1}$, which comes from the orthogonality of \mathbf{U} . This equation can be written componentwise as

$$[\mathbf{U}^\top \boldsymbol{\omega}]_i = -\lambda_i [\mathbf{U}^\top \delta\boldsymbol{\phi}]_i. \quad (\text{A8})$$

For $i = 1$, Eq. (A8) can be written as $\sum_j \omega_j = -\lambda_1 \sum_j \delta\phi_j$. Therefore, $\sum_j \delta\phi_j$ can have any value because $\sum_j \omega_j = 0$ and $\lambda_1 = 0$. This property might be given by the singularity of \mathbf{J} . We use constraint $\sum_j \delta\phi_j = 0$ for later use. In fact, we checked whether $\boldsymbol{\omega} = -\mathbf{J}\delta\boldsymbol{\phi}$ is solvable by using the pseudo-inverse property of \mathbf{J} , with the result giving a comparable solution with the numerical data under this constraint.

For $i > 1$ with $\lambda_i \neq 0$, Eq. (A8) can be transformed into $-[\mathbf{U}^\top \boldsymbol{\omega}]_i / \lambda_i = [\mathbf{U}^\top \delta\boldsymbol{\phi}]_i$. By using $\delta\boldsymbol{\phi}^\top \delta\boldsymbol{\phi} = (\mathbf{U}^\top \delta\boldsymbol{\phi})^\top (\mathbf{U}^\top \delta\boldsymbol{\phi})$, we can derive the relation between $s_{\delta\phi}$ and $\boldsymbol{\omega}$ as

$$\begin{aligned} s_{\delta\phi} &= \sqrt{\frac{1}{N} \sum_{i=1}^N \delta\phi_i^2} \\ &= \sqrt{\frac{1}{N} \sum_{i=1}^N [\mathbf{U}^\top \delta\boldsymbol{\phi}]_i^2} \\ &= \frac{1}{\sqrt{N}} \sqrt{\sum_{i=2}^N \frac{1}{\lambda_i^2} [\mathbf{U}^\top \boldsymbol{\omega}]_i^2 + \frac{1}{N} \left(\sum_{i=1}^N \delta\phi_i \right)^2} \\ &= \frac{1}{\sqrt{N}} \sqrt{\sum_{i=2}^N \frac{1}{\lambda_i^2} [\mathbf{U}^\top \boldsymbol{\omega}]_i^2}. \end{aligned} \quad (\text{A9})$$

For the last step, we use the constraint $\sum_{i=1}^N \delta\phi_i = 0$.

For an arbitrary random permutation $\tilde{\sigma}$ in Sec. IV, we change s_ω for a fixed $\tilde{\sigma}$. Then, $\boldsymbol{\omega}$ is a function of $\tilde{\sigma}$ and s_ω given by $\boldsymbol{\omega}(\tilde{\sigma}, s_\omega) = s_\omega \boldsymbol{\omega}(\tilde{\sigma}, 1)$. If we average Eq. (A9) over all permutations $\tilde{\sigma}$, the righthand side is represented as

$$\begin{aligned} s_{\delta\phi} &= \frac{1}{\sqrt{N}} \left\langle \sqrt{\sum_{j=2}^N \frac{1}{\lambda_j^2} [\mathbf{U}^\top \boldsymbol{\omega}(\tilde{\sigma}, s_\omega)]_j^2} \right\rangle_{\tilde{\sigma}} \\ &= \frac{1}{\sqrt{N}} \left\langle \sqrt{\sum_{j=2}^N \frac{1}{\lambda_j^2} [\mathbf{U}^\top s_\omega \boldsymbol{\omega}(\tilde{\sigma}, 1)]_j^2} \right\rangle_{\tilde{\sigma}} \\ &= \frac{s_\omega}{\sqrt{N}} \left\langle \sqrt{\sum_{j=2}^N \frac{1}{\lambda_j^2} [\mathbf{U}^\top \boldsymbol{\omega}(\tilde{\sigma}, 1)]_j^2} \right\rangle_{\tilde{\sigma}} \propto \frac{s_\omega}{K} \end{aligned} \quad (\text{A10})$$

for fixed N . Ultimately, we use $\lambda_i = K \bar{\lambda}_i$ for $\forall i$ where $\bar{\lambda}_i$ is the i th eigenvalue of \mathbf{J} for $K = 1$. Accordingly, we derived the relation $s_{\delta\phi} \propto s_\omega/K$, which we numerically checked as shown in Fig. 5.

- [1] S. H. Strogatz, *Sync* (Hyperion, New York, 2003).
- [2] A. Pikovsky, M. Rosenblum, and J. Kurths, *Synchronization: A Universal Concept in Nonlinear Sciences* (Cambridge University Press, Cambridge, 2001).
- [3] T. J. Walker, *Science* **166**, 891 (1969).
- [4] C. Liu, D. R. Weaver, S. H. Strogatz, and S. M. Reppert, *Cell* **91**, 855 (1997).
- [5] F. Varela, J.-P. Lachaux, E. Rodriguez, and J. Martinerie, *Nat. Rev. Neurosci.* **2**, 229 (2001).
- [6] A. K. Engel, P. Fries, and W. Singer, *Nat. Rev. Neurosci.* **2**, 704 (2001).
- [7] Z. Jiang and M. McCall, *J. Opt. Soc. Am. B* **10**, 155 (1993).
- [8] S. Yu. Kourtchatov, V. V. Likhanskii, A. P. Napartovich, F. T. Arecchi, and A. Lapucci, *Phys. Rev. A* **52**, 4089 (1995).
- [9] A. E. Motter, S. A. Myers, M. Anghel, and T. Nishikawa, *Nat. Phys.* **9**, 191 (2013).
- [10] G. Filatrella, A. H. Nielsen, and N. F. Pedersen, *Eur. Phys. J. B* **61**, 485 (2008).
- [11] Z. Nédá, E. Ravasz, Y. Brechet, T. Vicsek, and A.-L. Barabási, *Nature (London)* **403**, 849 (2000).
- [12] K. Wiesenfeld, P. Colet, and S. H. Strogatz, *Phys. Rev. Lett.* **76**, 404 (1996).
- [13] J. D. Crawford, *J. Stat. Phys.* **74**, 1047 (1994); *Phys. Rev. Lett.* **74**, 4341 (1995); J. D. Crawford and K. T. R. Davies, *Physica D (Amsterdam)* **125**, 1 (1999).
- [14] A. Arenas, A. D.-Guilera, J. Kurths, Y. Moreno, and C. Zhou, *Phys. Rep.* **469**, 93 (2008).
- [15] Y. Kuramoto, in *Proceedings of the International Symposium on Mathematical Problems in Theoretical Physics*, edited by H. Araki, Lecture Notes in Physics Vol. 39 (Springer, New York, 1975), pp. 420–422; Y. Kuramoto and I. Nishikawa, *J. Stat. Phys.* **49**, 569 (1987).
- [16] J. A. Acebrón, L. L. Bonilla, C. J. Pérez Vicente, and F. Ritort, *Rev. Mod. Phys.* **77**, 137 (2005).
- [17] H. Hong, H. Park, and M. Y. Choi, *Phys. Rev. E* **72**, 036217 (2005).
- [18] D. A. Wiley, S. H. Strogatz, and M. Girvan, *Chaos* **16**, 015103 (2006).
- [19] R. Delabays, M. Tyloo, and P. Jacquod, *Chaos* **27**, 103109 (2017).
- [20] J. A. Rogge and D. Aeyels, *J. Phys. A* **37**, 11135 (2004).
- [21] R. Delabays, T. Coletta, and P. Jacquod, *J. Math. Phys.* **57**, 032701 (2016).
- [22] J. Ochab and P. F. Góra, *Acta Phys. Pol. B Proc. Suppl.* **3**, 453 (2010).
- [23] R. Delabays, T. Coletta, and P. Jacquod, *J. Math. Phys.* **58**, 032703 (2017).
- [24] D. Manik, M. Timme, and D. Witthaut, *Chaos* **27**, 083123 (2017).
- [25] A. Marsden, *Eigenvalues of the Laplacian and Their Relationship to the Connectedness of a Graph* (University of Chicago Press, Chicago, 2013).
- [26] F. R. K. Chung, *Spectral Graph Theory* (American Mathematical Society, Providence, RI, 1997).
- [27] P. J. Menck, J. Heitzig, N. Marwan, and J. Kurths, *Nat. Phys.* **9**, 89 (2013).
- [28] R. E. Mirollo, *SIAM J. Math. Anal.* **25**, 1176 (1994).
- [29] V. Nicosia, M. Valencia, M. Chavez, A. Díaz-Guilera, and V. Latora, *Phys. Rev. Lett.* **110**, 174102 (2013).
- [30] L. M. Pecora, F. Sorrentino, A. M. Hagerstrom, T. E. Murphy, and R. Roy, *Nat. Commun.* **5**, 4079 (2014).
- [31] F. Sorrentino, L. M. Pecora, A. M. Hagerstrom, T. E. Murphy, and R. Roy, *Sci. Adv.* **2**, e1501737 (2016).
- [32] Y. S. Cho, T. Nishikawa, and A. E. Motter, *Phys. Rev. Lett.* **119**, 084101 (2017).
- [33] H. Hong, H. Chaté, L.-H. Tang, and H. Park, *Phys. Rev. E* **92**, 022122 (2015).